Electronic Supplementary Information

Complexation properties of *N*-thiophosphorylated thiourea 2-PyNHC(S)NHP(S)(O*i*Pr)$_2$ towards Ni^{II}

Damir A. Safin,*[a] Maria G. Babashkina,[a] Piotr Kubisiak,[b] Mariusz P. Mitoraj,*[b] Koen Robeyns[a], Etienne Goovaerts*[c] and Yann Garcia*[a]

[a] *Institute of Condensed Matter and Nanosciences, MOST - Inorganic Chemistry, Université Catholique de Louvain, Place L. Pasteur 1, 1348 Louvain-la-Neuve, Belgium. Fax: +32(0) 1047 2330; Tel: +32(0) 1047 2831; E-mail: damir.safin@ksu.ru, yam.garcia@uclouvain.be*

[b] *Department of Theoretical Chemistry, Faculty of Chemistry, Jagiellonian University, R. Ingardena 3, 30-060 Cracow, Poland. E-mail: mitoraj@chemia.uj.edu.pl.*

[c] *Physics Department, University of Antwerp, Universiteitsplein 1, 2610 Antwerpen, Belgium; E-mail: etienne.goovaerts@ua.ac.be*

Physical measurements: Infrared spectra were recorded with a Thermo Nicolet 380 FT-IR spectrometer in the range 400–3600 cm^{-1}. NMR spectra were obtained on a Bruker Avance 300 MHz spectrometer at 25 °C. ^{1}H and ^{31}P{^{1}H} NMR spectra in $CDCl_3$ and DMSO-d_6 were recorded at 299.948 and 121.420 MHz, respectively. Chemical shifts are reported with reference to $SiMe_4$ (^{1}H) and 85% H_3PO_4 (^{31}P{^{1}H}). The UV-vis/NIR absorption spectrum in 10^{-4} M solution in CH_2Cl_2 was recorded on a Lambda-35 spectrometer in the range 200–1000 nm. Elemental analyses were performed on a Thermoquest Flash EA 1112 Analyzer from CE Instruments. Continuous wave EPR measurements were performed in a W-band EPR spectrometer (Bruker Elexsys E680) equipped with standard cylindrical cavity and liquid helium cooled cryostat. EPR measurement parameters: microwave frequency 94.0 GHz, microwave power 44 μW, field modulation at 100 kHz with amplitude 0.8 mT. Background subtraction was performed to eliminate spurious signals from the empty resonator and an eventual background drift. For clarity of presentation a narrow region has been omitted containing g ≈ 2 signals not related to the studied complex. The crystallites of **[Ni(L-1,5,7-*N*,*N*′,*S*)$_2$]** were grown from acetone/*n*-hexane solution and visually selected for best morphology for the EPR experiments, but were found to be polycrystalline from control measurements by X-ray diffraction. The anisotropic EPR resonances are then originating from a larger single crystal area in the sample.

Synthesis of the [NiL$_2$] complex: A suspension of **HL** (0.667 g, 2 mmol) in aqueous methanol (20 mL) was mixed with a methanol solution of potassium hydroxide (0.123 g, 2.2 mmol). An aqueous (20 mL) solution of $NiCl_2$ (0.127 g, 1 mmol) was added dropwise under vigorous stirring to the resulting potassium salt. The mixture was stirred at room temperature for 3 h and left overnight. The resulting complex was extracted with

dichloromethane, washed with water and dried with anhydrous $MgSO_4$. The solvent was then removed in vacuo. Yield: 0.665 g (92 %). IR (Nujol; ν, cm^{-1}): 573 (P=S), 976 (POC), 1531 (SCN), 1610 (Py), 3211 (NH). IR (CH_2Cl_2; ν, cm^{-1}): 611 (P=S), 982 (POC), 1548 (SCN), 1619 (Py), 3224 (NH). UV-vis (CH_2Cl_2), [λ_{max}, nm (ε, M^{-1} cm^{-1})]: 302 (31842), 682 (217), 731 (269), 792 (198). $C_{24}H_{38}N_6NiO_4P_2S_4$ (723.48): calcd. C 39.84, H 5.29, N 11.62; found: C 39.71, H 5.34, N 11.53 %.

DFT calculations: We have applied in DFT-based geometry optimizations the hybrid exchange-correlation functional B3LYP[1,2] and the LANL2DZ basis set by Wadt and Hay,[3] as implemented in the Gaussian 09 package.[4] Additionally, the 6-31G** basis set was also applied for the selected complexes. In order to include the solvent effects the Polarized Continuum Model (PCM) was used.[5] UV-vis spectra based on the TD-DFT method (at the level of B3LYP/TZP) and the EPR g-tensor values (at the level of BP86/TZP) were calculated by the ADF2009.01 package.[6,7] Molecular orbitals and TD-DFT spectra were plotted with the ADF-GUI 2009.01 interface.[8]

X-Ray crystallography: The X-ray data for **[Ni(L-1,5,7-*N*,*N*′,*S*)$_2$]·CH_2Cl_2** were collected on a STOE IPDS-II diffractometer with graphite-monochromatised Mo-K_α radiation generated by a fine-focus X-ray tube operated at 50 kV and 40 mA. The reflections of the images were indexed, integrated and scaled using the X-Area data reduction package.[9] Data were corrected for absorption using the PLATON program.[10] The structures were solved by direct methods using the SHELXS-97 program[11] and refined first isotropically and then anisotropically using SHELXL-97.[11] Hydrogen atoms were revealed from $\Delta\rho$ maps and those bonded to C were refined using appropriate riding models. H atoms bonded to N were freely refined. The structure of **[Ni(L-1,5,7-*N*,*N*′,*S*)$_2$]·CH_2Cl_2** shows two independent molecules in the asymmetric unit of the triclinic *P*–1 unit cell.

The X-ray data for **[Ni(L-1,5,7-*N*,*N*′,*S*)$_2$]** were collected on a MAR345 image plate, with Mo-K_α radiation (Zr filter) generated by a Rigaku UltraX 18 rotating anode. The reflections of the images were indexed and integrated using the CrysalisPro package (Agilent Technologies).[12] Data were scaled and corrected for absorption using the integrated scale3 abspack procedure. The structures were solved by direct methods (SHELXS-97)[11] and refined first isotropically and then anisotropically using SHELXL-97.[11] Hydrogen atoms were placed at calculated positions and refined in riding mode with respect to the parent atoms. For **[Ni(L-1,5,7-*N*,*N*′,*S*)$_2$]**, crystals diffracted poorly (about 1.2 Å) and although all the data were used for structure solution (SHELXS), data were limited to 1.4 Å for refinement. Moreover the crystals appeared to be twinned (180° around the direct b-axis) and were processed accordingly, giving a HKLF 5 formatted reflection file and a refined BASF factor of 50.2%. The ligands were refined using a full set of bond and some angle restraints. The interactions with the Ni atom are not subjected to any restraints. The large number of parameters (Z' = 4) against the small number of data points (low resolution), twinning, and incorrectness of the model due to the

inability to describe the flexibility of the isopropyl moieties results in the high R, ωR_2 values. Moreover the large (207 Å^3) cavity could not be corrected for by the Platon squeeze method, as this only works on HKLF 4 formatted datasets. A pseudo-translation peak is present at 0 0.5 0, providing indirect prove of the thermal phase transition between the two reported forms of **[Ni(L-1,5,7-*N*,*N*′,*S*)$_2$]**.

Figures were generated using the program Mercury.[13]

Crystal data for [Ni(L-1,5,7-*N*,*N*′,*S*)$_2$]·CH$_2$Cl$_2$: $C_{24}H_{38}N_6NiO_4P_2S_4$, CH_2Cl_2, M_r = 808.42 g mol^{-1}, triclinic, space group P–1, a = 11.5622(6), b = 16.9673(8), c = 20.7405(9) Å, α = 85.690(4), β = 82.885(4), γ = 71.258(4)°, V = 3820.7(3) Å^3, Z = 4, ρ = 1.406 g cm^{-3}, μ(Mo-Kα) = 0.988 mm^{-1}, T = 173 K, reflections: 36183 collected, 14806 unique, R_{int} = 0.096, R_1(all) = 0.0775, wR_2(all) = 0.2323.

Crystal data for [Ni(L-1,5,7-*N*,*N*′,*S*)$_2$]: $C_{24}H_{38}N_6NiO_4P_2S_4$, M_r = 723.49 g mol^{-1}, triclinic, space group P–1, a = 12.7488(11), b = 19.4527(16), c = 30.933(3) Å, α = 73.231(7), β = 81.966(7), γ = 89.965(7)°.

CCDC 821199 (**[Ni(L-1,5,7-*N*,*N*′,*S*)$_2$]·CH$_2$Cl$_2$**) contains the supplementary crystallographic data. These data can be obtained free of charge via http://www.ccdc.cam.ac.uk/conts/retrieving.html, or from the Cambridge Crystallographic Data Centre, 12 Union Road, Cambridge CB2 1EZ, UK; fax: (+44) 1223-336-033; or e-mail: deposit@ccdc.cam.ac.uk.

References

1 J. P. Perdew, *Phys. Rev. B: Condens. Matter*., 1986, **33**, 8822.

2 A. D. Becke, *J. Chem. Phys.*, 1993, **98**, 1372.

3 P. J. Hay and W. R. Wadt, *J. Chem. Phys.*, 1985, **82**, 270.

4 M. J. Frisch, G. W. Trucks, H. B. Schlegel, G. E. Scuseria, M. A. Robb, J. R. Cheeseman, G. Scalmani, V. Barone, B. Mennucci, G. A. Petersson, H. Nakatsuji, M. Caricato, X. Li, H. P. Hratchian, A. F. Izmaylov, J. Bloino, G. Zheng, J. L. Sonnenberg, M. Hada, M. Ehara, K. Toyota, R. Fukuda, J. Hasegawa, M. Ishida, T. Nakajima, Y. Honda, O. Kitao, H. Nakai, T. Vreven, J. A. Montgomery Jr., J. E. Peralta, F. Ogliaro, M. Bearpark, J. J. Heyd, E. Brothers, K. N. Kudin, V. N. Staroverov, R. Kobayashi, J. Normand, K. Raghavachari, A. Rendell, J. C. Burant, S. S. Iyengar, J. Tomasi,M. Cossi, N. Rega, J. M. Millam, M. Klene, J. E. Knox, J. B. Cross, V. Bakken, C. Adamo, J. Jaramillo, R. Gomperts, R. E. Stratmann, O. Yazyev, A. J. Austin, R. Cammi, C. Pomelli, J. W. Ochterski, R. L. Martin, K. Morokuma, V. G. Zakrzewski, G. A. Voth, P. Salvador, J. J. Dannenberg, S. Dapprich, A. D. Daniels, Ö. Farkas, J. B. Foresman, J. V. Ortiz, J. Cioslowski and D. J. Fox, Gaussian 09, Gaussian Inc., Wallingford CT, 2009.

5 J. Tomasi, B. Mennucci, R. Cammi *Chem. Rev.*, 2005, **105**, 2999.

6 G. te Velde, F. M. Bickelhaupt, E. J. Baerends, C. Fonseca Guerra, S. J. A. van Gisbergen, J. G. Snijders and T. Ziegler, *J. Comput. Chem.*, 2001, **22**, 931 and references therein.

7 E. J. Baerends, J. Autschbach, D. Bashford, A. Bérces, F. M. Bickelhaupt, C. Bo, P. M. Boerrigter, L. Cavallo, D. P. Chong, L. Deng, R. M. Dickson, D. E. Ellis, M. van Faassen, L. Fan, T. H. Fischer, C. Fonseca Guerra, A. Ghysels, A. Giammona, S. J. A. van Gisbergen, A. W. Götz, J. A. Groeneveld, O. V. Gritsenko, M. Grüning, F. E. Harris, P. van den Hoek, C. R. Jacob, H. Jacobsen, L. Jensen, G. van Kessel, F. Kootstra, M. V. Krykunov, E. van Lenthe, D. A. McCormack, A. Michalak, M. Mitoraj, J. Neugebauer, V. P. Nicu, L. Noodleman, V. P. Osinga, S. Patchkovskii, P. H. T. Philipsen, D. Post, C. C. Pye, W. Ravenek, J. I. Rodríguez, P. Ros, P. R. T. Schipper, G. Schreckenbach, M. Seth, J. G. Snijders, M. Solà, M. Swart, D. Swerhone, G. te Velde, P. Vernooijs, L. Versluis, L. Visscher, O. Visser, F. Wang, T. A. Wesolowski, E. M. van Wezenbeek, G. Wiesenekker, S. K. Wolff, T. K. Woo, A. L. Yakovlev and T. Ziegler, Theoretical Chemistry; Vrije Universiteit: Amsterdam.

8 ADF-GUI 2009.01, SCM, Amsterdam, The Netherlands, http://www.scm.com (O. Visser, P. Leyronnas, W.-J. van Zeist and M. Lupki).

9 Stoe & Cie. X-AREA. Area-Detector Control and Integration Software. Stoe & Cie, Darmstadt, Germany, 2001.

10 A. L. Spek, *Acta Crystallogr.*, 2009, **D65**, 148.

11 G. M. Sheldrick, *Acta Crystallogr.*, 2008, **A64**, 112.

12 Agilent Technologies XRD (2010). Agilent Technologies, Xcalibur CCD system, CrysAlisPro Software system, Version 1.171.35.19

13 I. J. Bruno, J. C. Cole, P. R. Edgington, M. Kessler, C. F. Macrae, P. McCabe, J. Pearson and R. Taylor, *Acta Crystallogr.*, 2002, **B58**, 389.

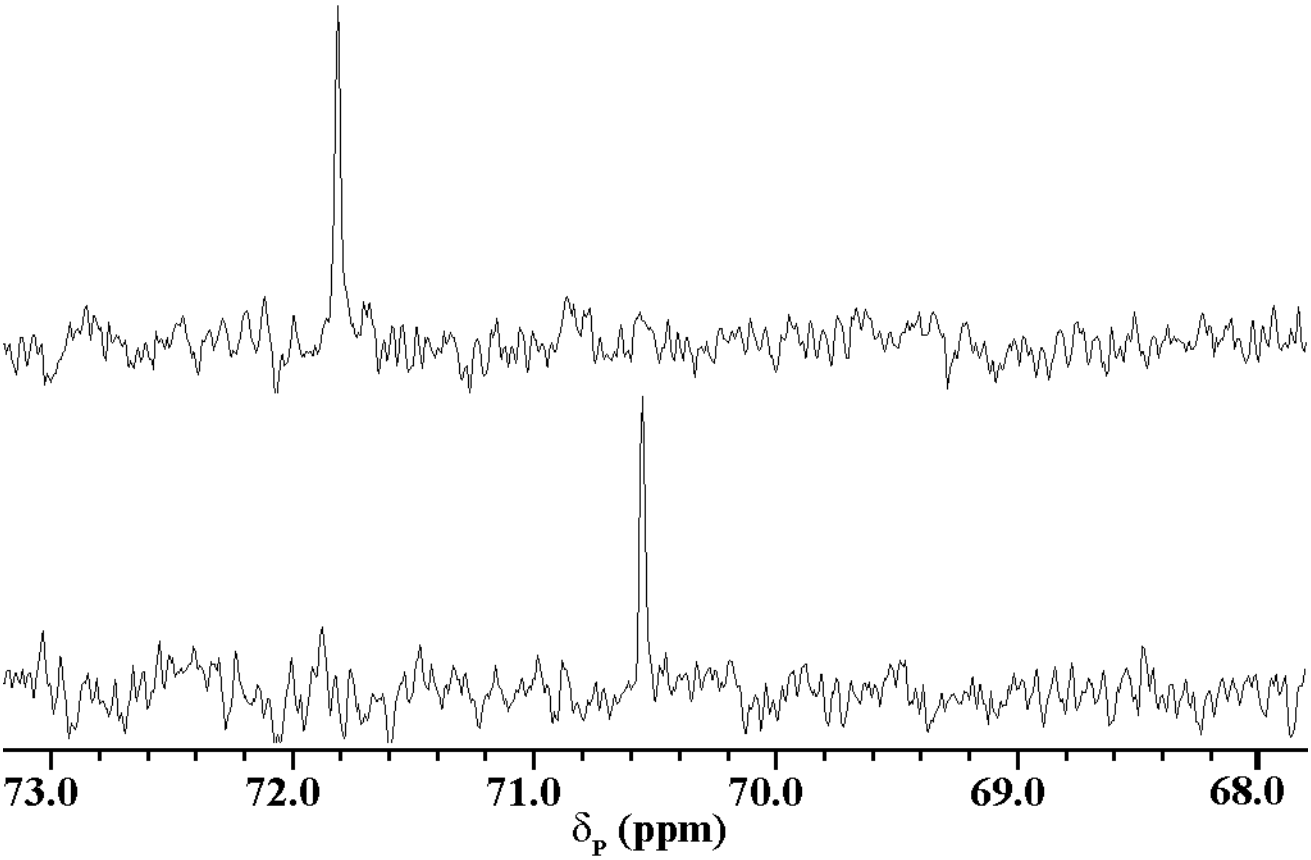

Fig. S1 $^{31}P\{^{1}H\}$ NMR spectra of **[NiL$_2$]** in $CDCl_3$ (bottom) and DMSO-d_6 (top).

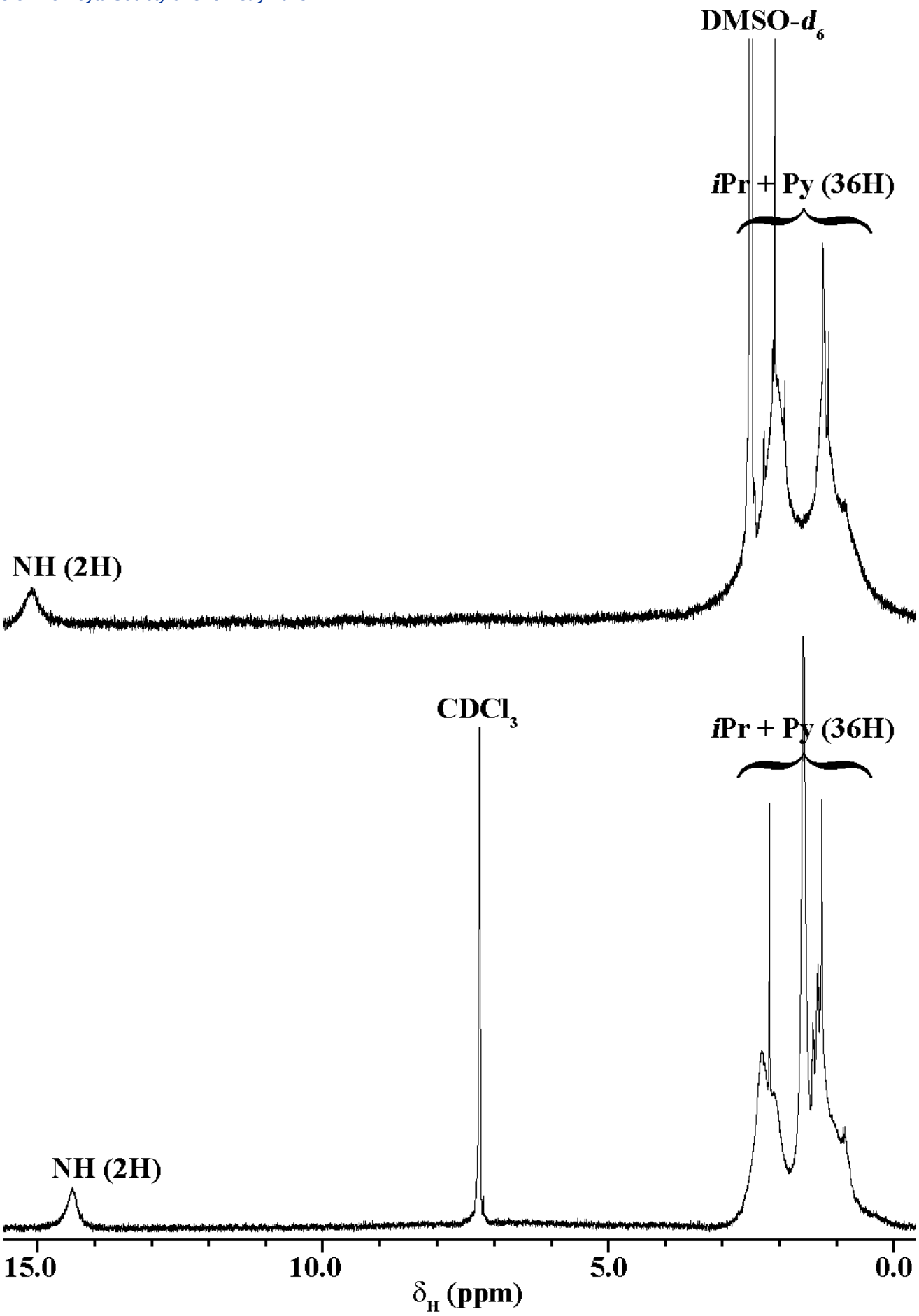

Fig. S2 ^{1}H NMR spectra of **[NiL$_2$]** in $CDCl_3$ (bottom) and DMSO-d_6 (top).

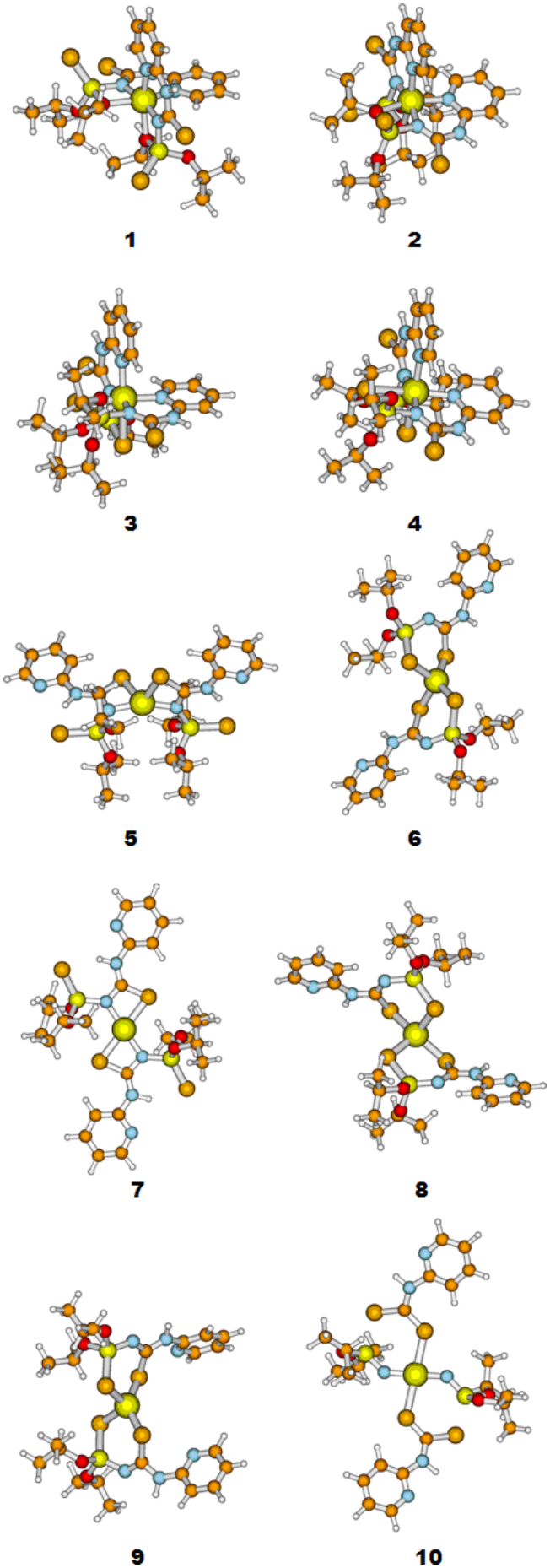

Fig. S3 Different structures of **[NiL$_2$]** as obtained from static density functional theory (DFT) based calculations, performed at the B3LYP level of theory.

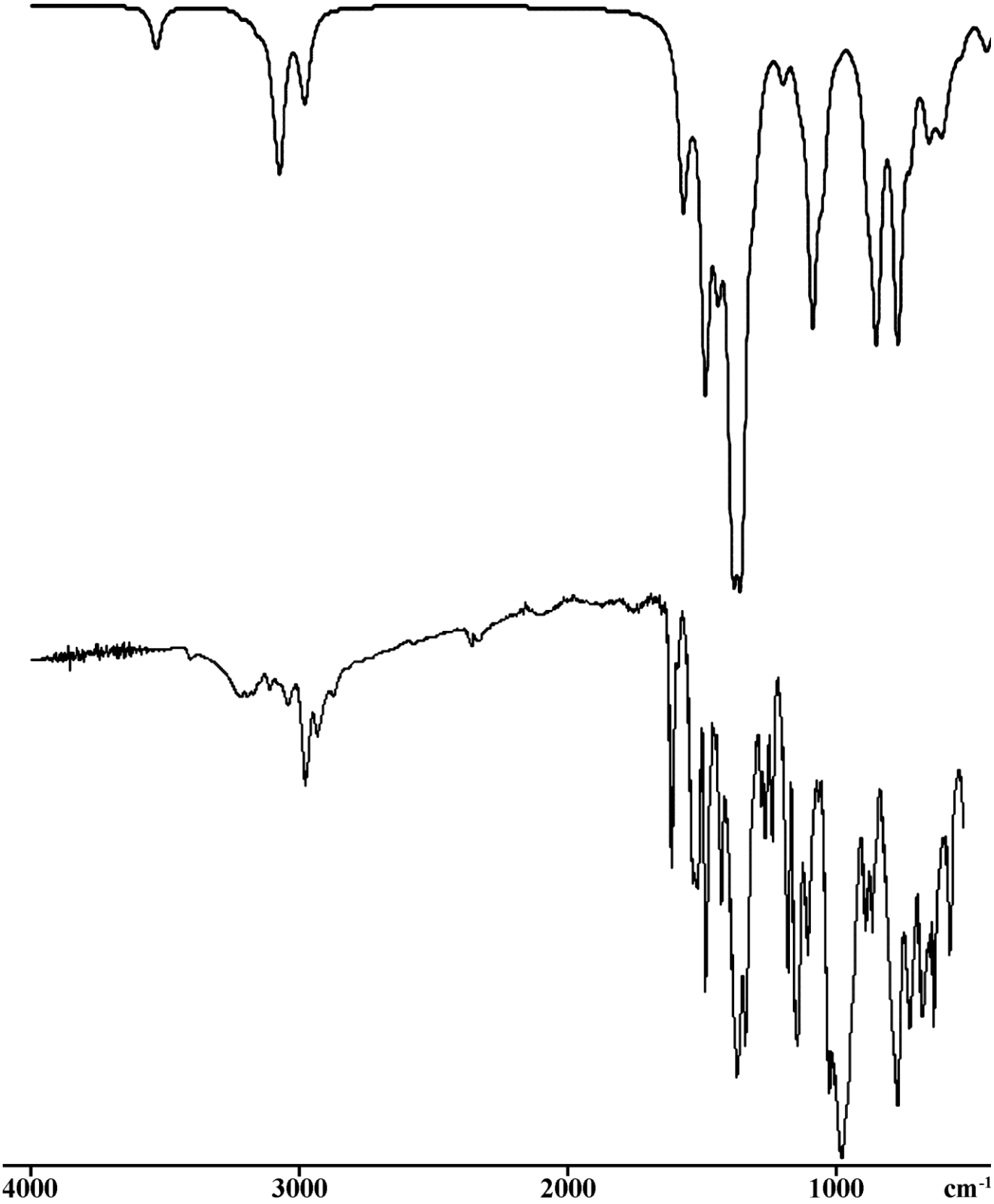

Fig. S4 Simulated (DFT/B3LYP, triplet **[NiL$_2$]**) (top) and experimental (bottom) IR spectra of **[NiL$_2$]**.

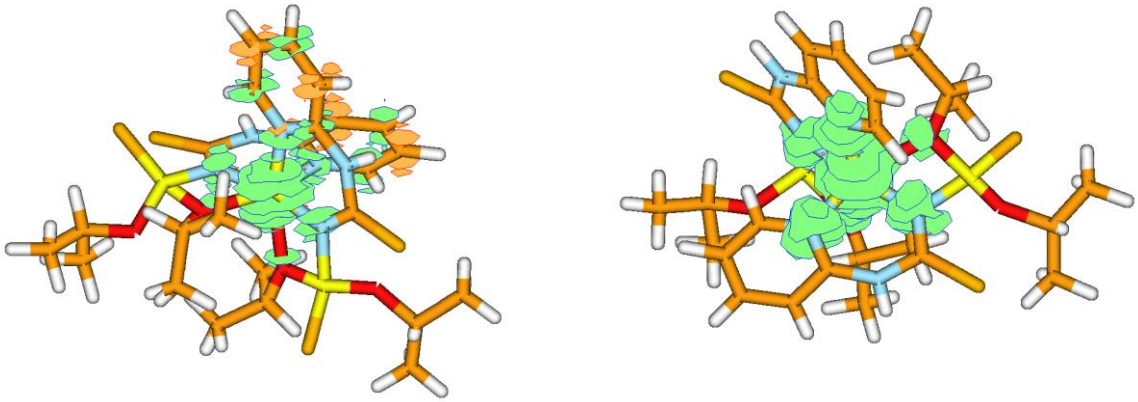

MP2 **DFT (B3LYP, similar was found for BP86)**

Fig. S5 Spin density (MP2 and DFT calculations) of the **[NiL$_2$]** triplet (green color shows the alpha electron density).

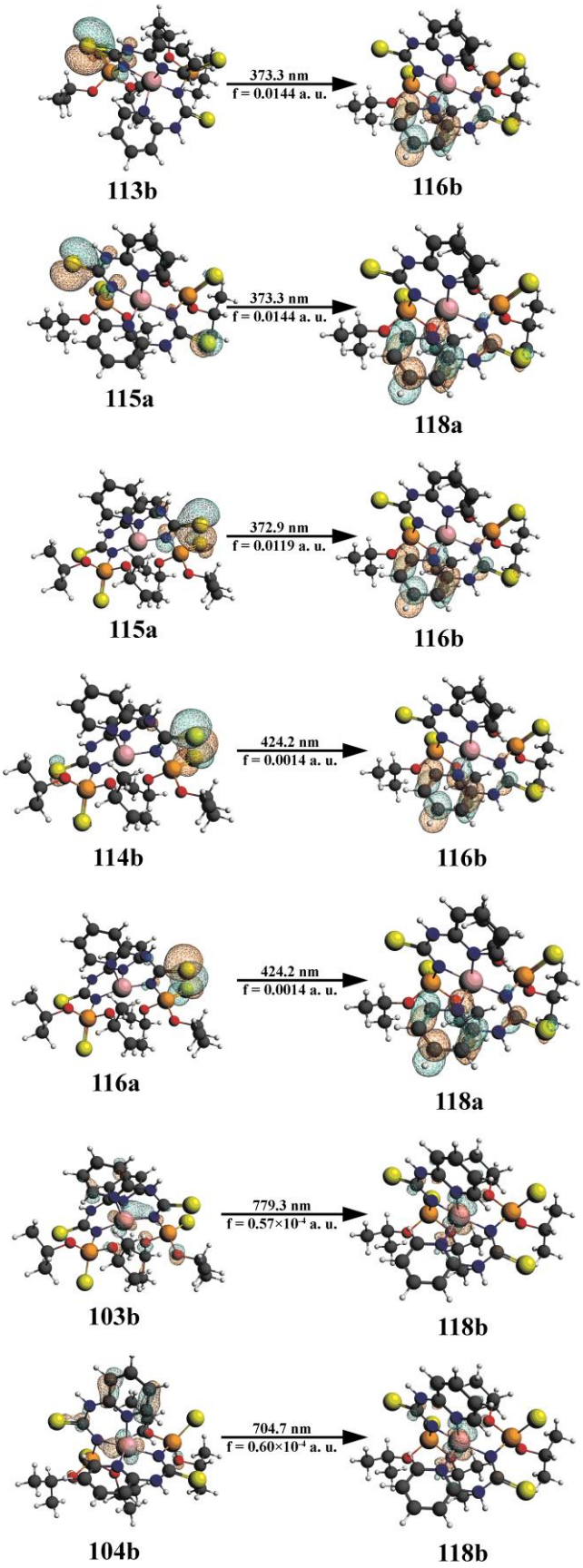

Fig. S6 The contrours of molecular orbitals involved in the dominant transitions.

Table S1 Selected bond lengths (Å) and bond angles (°) for **[Ni(L-1,5,7-*N*,*N*′,*S*)$_2$]·CH$_2$Cl$_2$**

Molecule **A**		Molecule **B**	
Bond lengths			
Ni(1)–N(1)	2.018(5)	Ni(2)–N(7)	2.025(5)
Ni(1)–N(3)	2.068(5)	Ni(2)–N(9)	2.037(5)
Ni(1)–N(4)	2.025(4)	Ni(2)–N(10)	2.014(5)
Ni(1)–N(6)	2.062(5)	Ni(2)–N(12)	2.086(5)
Ni(1)–S(2)	2.5886(18)	Ni(2)–S(6)	2.6469(16)
Ni(1)–S(4)	2.6512(17)	Ni(2)–S(8)	2.5976(17)
C(1)–N(1)	1.358(7)	C(25)–N(7)	1.344(7)
C(1)–N(2)	1.359(7)	C(25)–N(8)	1.376(7)
C(1)–S(1)	1.689(6)	C(25)–S(1)	1.686(6)
C(13)–N(4)	1.323(9)	C(37)–N(10)	1.355(7)
C(13)–N(5)	1.377(8)	C(37)–N(11)	1.377(7)
C(13)–S(3)	1.690(6)	C(37)–S(7)	1.690(6)
P(1)–N(1)	1.653(5)	P(3)–N(7)	1.642(5)
P(1)–S(2)	1.962(2)	P(3)–S(6)	1.964(2)
P(2)–N(4)	1.650(5)	P(4)–N(10)	1.652(5)
P(2)–S(4)	1.965(2)	P(4)–S(8)	1.957(2)
Bond angles			
Ni(1)–N(1)–C(1)	129.0(4)	Ni(2)–N(7)–C(25)	127.9(4)
Ni(1)–N(4)–C(13)	129.0(4)	Ni(2)–N(10)–C(37)	130.7(4)
Ni(1)–N(1)–P(1)	103.8(2)	Ni(2)–N(7)–P(3)	104.8(3)
Ni(1)–N(4)–P(2)	104.7(3)	Ni(2)–N(10)–P(4)	104.3(2)
Ni(1)–S(2)–P(1)	77.76(7)	Ni(2)–S(6)–P(3)	76.82(7)
Ni(1)–S(4)–P(2)	76.87(7)	Ni(2)–S(8)–P(4)	77.81(7)
N(1)–Ni(1)–N(3)	90.48(19)	N(7)–Ni(2)–N(9)	89.24(18)
N(1)–Ni(1)–N(4)	164.7(2)	N(7)–Ni(2)–N(10)	163.17(19)
N(1)–Ni(1)–N(6)	101.46(18)	N(7)–Ni(2)–N(12)	104.18(19)
N(3)–Ni(1)–N(4)	100.5(2)	N(9)–Ni(2)–N(10)	99.66(18)
N(3)–Ni(1)–N(6)	87.72(19)	N(9)–Ni(2)–N(12)	92.96(19)
N(4)–Ni(1)–N(6)	89.73(19)	N(10)–Ni(2)–N(12)	89.70(19)
S(2)–Ni(1)–N(1)	74.93(14)	S(6)–Ni(2)–N(7)	74.00(14)
S(2)–Ni(1)–N(3)	164.74(13)	S(6)–Ni(2)–N(9)	161.46(14)
S(2)–Ni(1)–N(4)	94.70(16)	S(6)–Ni(2)–N(10)	98.57(13)

S(2)–Ni(1)–N(6)	90.78(14)	S(6)–Ni(2)–N(12)	83.74(13)
S(2)–Ni(1)–S(4)	98.44(6)	S(6)–Ni(2)–S(8)	96.64(6)
S(4)–Ni(1)–N(1)	96.01(14)	S(8)–Ni(2)–N(7)	91.02(14)
S(4)–Ni(1)–N(3)	87.35(13)	S(8)–Ni(2)–N(9)	91.46(14)
S(4)–Ni(1)–N(4)	74.07(15)	S(8)–Ni(2)–N(10)	74.62(14)
S(4)–Ni(1)–N(6)	161.88(13)	S(8)–Ni(2)–N(12)	164.22(14)

Table S2 Hydrogen bond and hydrogen contact lengths (Å) and angles (°) for **[Ni(L-1,5,7-*N*,*N*′,*S*)$_2$]·CH$_2$Cl$_2$**[a]

D–H···A	*d*(D–H)	*d*(H···A)	*d*(D···A)	∠(DHA)
N(2)–H(1)···S(1)#1	0.88	2.66	3.514(5)	164
N(5)–H(1A)···S(5)	0.88	2.53	3.359(5)	158
N(8)–H(1B)···S(3)	0.88	2.49	3.321(5)	157
N(11)–H(1C)···S(7)#2	0.88	2.57	3.430(5)	167

[a] Symmetry transformations used to generate equivalent atoms: #1: 2 – *x*, –*y*, 1 – *z*; #2: 1 – *x*, 2 – *y*, 2 – *z*.

Table S3 Relative energies of the structures **1–10**, shown on Fig. S3 and given with respect to the most stable triplet species **1** (DFT/B3LYP/LanL2DZ).

Structure	Triplet	Singlet	Quintet
1	0.0	37.4	72.8
2	11.3	39.3	
3	13.6	37.4	
4	15.2	37.4	
5	36.3	27.0	
6	39.1	23.7	
7	40.2	-0.6	
8	40.8	26.1	
9	59.5	21.8	
10	130.1	15.8	

Table S4 Relative energies (DFT/B3LYP/6-31G**) of the lowest energy triplet structures **1–4**, shown on Fig. S3, in the gas phase and in the CH_2Cl_2 solvent (included at the PCM level of theory).

Structure	Gas phase	PCM model[a]	PCM model[a]
1	0.0	0.0	0.0
2	14.2	11.9	10.3
3[c]	4.0	6.4	3.4
4[c]	6.0	8.5	5.8

[a] Single point calculations based on the gas-phase geometries.

[b] Full geometry optimization including the PCM solvent model.

[c] Structures 3 and 4 correspond to the crystal units.